frontiers | Frontiers in Physics

TYPE Original Research
PUBLISHED 19 June 2023
DOI 10.3389/fphy.2023.1197726

OPEN ACCESS

EDITED BY
Valdir Guimaraes,
University of São Paulo, Brazil

REVIEWED BY
Vladimir Zelevinsky,
Michigan State University, United States
Maria Colonna,
Laboratori Nazionali del Sud (INFN), Italy
Pierre Descouvemont,
Université Libre de Bruxelles, Belgium

*CORRESPONDENCE
N. K. Timofeyuk,
n.timofeyuk@surrey.ac.uk

RECEIVED 31 March 2023
ACCEPTED 25 May 2023
PUBLISHED 19 June 2023

CITATION
Timofeyuk NK and Gómez-Ramos M (2023), Cluster scattering in the non-local model.
Front. Phys. 11:1197726.
doi: 10.3389/fphy.2023.1197726

Cluster scattering in the non-local model

N. K. Timofeyuk[1]* and M. Gómez-Ramos[2]

[1]Department of Physics, University of Surrey, Guildford, United Kingdom, [2]Departamento de FAMN, Universidad de Sevilla, Sevilla, Spain

Scattering of weakly bound nuclei with a pronounced cluster structure is strongly affected by their breakup. Usually, this mechanism is accounted for in a three-body model with pairwise potentials. The interaction potentials between complex systems are non-local due to the existence of excitation channels and antisymmetrization. However, a common practice is to use local optical potentials in cluster scattering studies. To assess the validity of replacing non-local optical potentials by their local equivalents, we extend the local-equivalent continuum-discretized coupled-channel (LECDCC) approach proposed by us for deuteron scattering in [Phys. Rev. C98, 011601(R) (2018)] to the case of cluster scattering. We consider the case of ^{6}Li + ^{120}Sn at 27 and 60 MeV, and compare the angular distributions and reaction cross sections for elastic and breakup cross sections with those obtained in the standard continuum-discretized coupled-channel (CDCC) method with local equivalents of non-local potentials. We found that while elastic scattering is not significantly affected by non-locality, the breakup observables could be affected by up to 20% depending on kinematical conditions of their observation.

KEYWORDS

three-body model, elastic scattering, breakup, continuum-discretized coupled-channel method, non-localities in optical potential

1 Introduction

The phenomenon of clustering has been known in nuclear physics for a long time. It is present in most light nuclei where two neutrons and two protons gain from gathering into an α-particle [1]. α-clustering also occurs in even–even $N = Z$ nuclei [2]. A special class of clustering, the halo nuclei, has been found around neutron and proton driplines [3]. More generally, clustering can occur in excited nuclear states close to the thresholds of particle emission channels. It influences cross sections of nuclear reactions involving them. Many such reactions are of importance for stellar nucleosynthesis [4], thus contributing much to shaping the world we live in.

Scattering of weakly bound nuclei with a pronounced cluster structure is at the frontier of modern experimental nuclear research [5, 6]. The information obtained from these studies is affected by the choice of theoretical models used to predict and/or analyze the measured observables. It has been known for a long time that theoretical models should include cluster breakup. To account for this important reaction mechanism, the scattering problem is often described in a three-body model with pairwise interactions, which are always chosen to be local. However, the general Feshbach theory states that interactions between complex systems are non-local [7]: they depend on the inter-nuclear separation both before and after collision. Non-locality comes both from removing the target excitation from consideration and from antisymmetrization between nucleons from both the target and projectile. It most naturally emerges in all *ab initio* calculations [8]. Therefore, an assessment

of validity of replacing non-local optical potentials by their local equivalents in cluster scattering calculations is a timely and vital task needed to correctly understand the uncertainties in observables due to optical potential choices.

We first note that two-body scattering with non-local interactions is very well studied. Phenomenological non-local potentials are often considered in the Perey–Buck model [9], for which the localization procedure has been established [9, 10]. Two-body scattering problems with non-local potentials of a general form can be treated easily by the R-matrix approach with a Lagrange mesh [11]. Many other methods of solving the non-local Schrödinger equation exist, examples of which, as well as references to other works, could be found in [12–14]. The solutions of two-body non-local scattering problems can be used to model wave functions both in the entrance and exit channels of various nuclear reactions when calculating their cross sections. Examples of such calculations are reviewed in [15] for the case of transfer reactions.

Three-body scattering problems with non-local potentials have been extensively studied for the case of three nucleons. They are usually solved either with the help of the Faddeev method [16, 17] or by using hyperspherical harmonics expansions [18, 19]. The Faddeev treatment of non-locality has also been extended to the case of deuteron scattering (d, d), transfer (d, p), and (p, d) reactions from heavy targets [20–22]. It was shown there that using local-equivalent nucleon-target potentials does not reproduce exact non-local calculations. Moreover, including non-locality in nucleon–target potentials significantly improves the description of experimental differential cross sections of these reactions as compared to those obtained in studies with local-equivalent nucleon optical potentials. These findings, together with the rapid development of microscopic models for optical potentials, have motivated the present study.

Modeling cluster scattering with non-local potentials requires a special theoretical technique. The Faddeev approach of [20–22] was applicable to (d, d) and (d, p) reactions because the two-body description of $n - A$ and $p - A$ bound states for the carefully selected target A works well. When applied for cluster scattering, Faddeev approach's requirement to achieve correct asymptotic conditions in all channels could be unachievable due to the complexity of the problem. In addition, there is no clarity in choosing two-body interaction potentials that would describe simultaneously bound and scattering states in the two-body subsystems. The normalization to unity of the two-body bound states in the Faddeev approach may not correspond to reality. For these reasons, we use the idea of [23], where the continuum-discretized coupled-channel (CDCC) approach [24, 25] was extended to provide an approximate three-body treatment of optical potentials' non-locality in the $n + p + A$ problem. Following [23], we derive a leading-order local-equivalent continuum-discretized coupled-channel (LECDCC) model for the case of scattering of nuclei with a well-pronounced two-cluster structure. We then compare the LECDCC predictions to those obtained in standard CDCC with local-equivalent potentials. We perform calculations for a popular choice of the projectile, ^{6}Li, which is well represented by the $\alpha - d$ cluster structure.

We start by formulating a three-body model for cluster scattering in Section 2, followed by developing LECDCC at the leading order in Section 3. In Section 4, we apply the formalism to the case of ^{6}Li + ^{120}Sn scattering using non-local Sao Paulo potentials [26–28] comparing LECDCC with traditional CDCC, in which local-equivalent potentials are used. Section 5 summarizes the work undertaken and draws conclusion. Appendix provides additional mathematical details relevant to formalism development.

2 Three-body model for cluster scattering

Let us consider scattering of the nucleus C composed by two clusters C_1 and C_2 from the target A. We assume that this problem can be well-described by the three-body wave function $\Psi(\boldsymbol{r}, \boldsymbol{R})$, which depends on coordinates $\boldsymbol{r} = \boldsymbol{r}_{C_1} - \boldsymbol{r}_{C_2}$ and $\boldsymbol{R} = \frac{C_1\boldsymbol{r}_{C_1} + C_2\boldsymbol{r}_{C_1}}{C_1 + C_2} - \boldsymbol{r}_A$, shown in Figure 1. We also assume that the interaction between any pair c of nuclei, chosen from C_1, C_2, and A, is described by a two-body Schrödinger equation:

$$\left(T_c + V_c^{coul}(\boldsymbol{r}_c) - E_c\right)\phi_c(\boldsymbol{r}_c) = -\int d\boldsymbol{r}_c' V_c(\boldsymbol{r}_c', \boldsymbol{r}_c)\phi_c(\boldsymbol{r}_c') \quad (1)$$

with non-local nuclear potential $V_c(\boldsymbol{r}_c', \boldsymbol{r}_c)$ and the local Coulomb interaction $V_c^{coul}(\boldsymbol{r}_c)$. The three-body Schrödinger equation in this case is written as follows (see Appendix for derivation):

$$\begin{aligned}&\left(T_r + T_R + V_{C_1A}^{coul}(\boldsymbol{R} + \gamma_1\boldsymbol{r}) + V_{C_2A}^{coul}(\boldsymbol{R} - \gamma_2\boldsymbol{r}) + V_{C_1C_2}^{coul}(\boldsymbol{r}) - E\right)\Psi(\boldsymbol{r}, \boldsymbol{R})\\ &= -\int d\boldsymbol{r}' V_{C_1C_2}(\boldsymbol{r}', \boldsymbol{r})\Psi(\boldsymbol{r}', \boldsymbol{R})\\ &\quad -\int d\boldsymbol{R}'\left[\mathcal{J}_1 V_{C_1A}\left(\boldsymbol{R}' + \gamma_1\boldsymbol{r} + \frac{\gamma_1\mu_C}{C_1}(\boldsymbol{R}' - \boldsymbol{R}), \boldsymbol{R} + \gamma_1\boldsymbol{r}\right)\Psi\left(\boldsymbol{r} + \frac{\mu_C}{C_1}(\boldsymbol{R}' - \boldsymbol{R}), \boldsymbol{R}'\right)\right.\\ &\quad \left.+\mathcal{J}_2 V_{C_2A}\left(\boldsymbol{R}' - \gamma_2\boldsymbol{r} + \frac{\gamma_2\mu_C}{C_2}(\boldsymbol{R}' - \boldsymbol{R}), \boldsymbol{R} - \gamma_2\boldsymbol{r}\right)\Psi\left(\boldsymbol{r} - \frac{\mu_C}{C_2}(\boldsymbol{R}' - \boldsymbol{R}), \boldsymbol{R}'\right)\right],\end{aligned} \quad (2)$$

where T_r and T_R are the kinetic energy operators associated with the coordinate r and R, respectively, $E = E_3 - E_{c.m.}$, where E_3 is the three-body energy in the laboratory system, while $\gamma_1 = C_2/(C_1 + C_2)$, $\gamma_2 = C_1/(C_1 + C_2)$, and $\mu_c = CA/(C + A)$. The two Jacobians are

$$\mathcal{J}_1 = \left(\frac{C}{C_1}\frac{A + C_1}{A + C}\right)^3, \quad \mathcal{J}_2 = \left(\frac{C}{C_2}\frac{A + C_2}{A + C}\right)^3. \quad (3)$$

We will assume for simplicity that the clusters and targets have zero spin. The three-body Schrödinger Eq. 2 is solved within the CDCC framework using the expansion

$$\Psi(\boldsymbol{r}, \boldsymbol{R}) = \sum_{i=1}^{n_{\max}} \chi_i(\boldsymbol{R})\phi_i(\boldsymbol{r}), \quad (4)$$

where ϕ_i is the $C_1 - C_2$ bound state wave function or a continuum bin, obtained in the non-local $C_1 - C_2$ model and χ_i is the wave function of the relative motion of the bin i with respect to the target A. It satisfies the equation

$$(T_R + U_C - E_i)\chi_i(\boldsymbol{R}) = -\sum_{i'}\int d\boldsymbol{R}' \mathcal{U}_{i'i}(\boldsymbol{R}', \boldsymbol{R})\chi_{i'}(\boldsymbol{R}'), \quad (5)$$

where U_C is the local $C - A$ Coulomb potential and

$$\mathcal{U}_{i'i}(\boldsymbol{R}',\boldsymbol{R}) = \int d\boldsymbol{r}\,\phi_{i'}(\boldsymbol{r})\Big[\mathcal{J}_1 V_{C_1A}\Big(\boldsymbol{R}'+\gamma_1\boldsymbol{r}+\frac{\gamma_1\mu_C}{C_1}(\boldsymbol{R}'-\boldsymbol{R}),\boldsymbol{R}+\gamma_1\boldsymbol{r}\Big)\phi_i\Big(\boldsymbol{r}+\frac{\mu_C}{C_1}(\boldsymbol{R}'-\boldsymbol{R})\Big) + \mathcal{J}_2 V_{C_2A}\Big(\boldsymbol{R}'-\gamma_2\boldsymbol{r}+\frac{\gamma_2\mu_C}{C_2}(\boldsymbol{R}'-\boldsymbol{R}),\boldsymbol{R}-\gamma_2\boldsymbol{r}\Big)\phi_i\Big(\boldsymbol{r}-\frac{\mu_C}{C_2}(\boldsymbol{R}'-\boldsymbol{R})\Big)\Big]. \tag{6}$$

In this paper, we will consider phenomenological non-local potentials in each pair c choosing them in the Perey–Buck form [9],

$$V(\boldsymbol{r},\boldsymbol{r}') = H_i(\boldsymbol{x})U_i(\boldsymbol{X}), \tag{7}$$

where $\boldsymbol{x} = \boldsymbol{r} - \boldsymbol{r}'$ and $\boldsymbol{X} = (\boldsymbol{r} + \boldsymbol{r}')/2$, and

$$H(\boldsymbol{x}) = \pi^{-3/2}\beta^{-3}\exp\left(-\frac{\boldsymbol{x}^2}{\beta^2}\right), \tag{8}$$

where β is the range of non-locality.

Usually, the non-locality range β for nucleon scattering is around 0.85–0.9 fm; for deuterons, it is ~ 0.54 fm, and for α-particles, it is ~ 0.25 fm. This is because in most cases, the clusters C_1 and C_2 are not the same, and different non-locality ranges are required in each pair c. Moreover, non-local potentials themselves could be represented by several terms of the Perey–Buck type with different non-locality ranges, such as in the non-local dispersive optical model (NLDOM) in [29]. Therefore, we consider pairwise potentials given by

$$V_c(\boldsymbol{r}_c',\boldsymbol{r}_c) = \sum_j H_j(\boldsymbol{x}_c)U_j^{(c)}(X_c), \tag{9}$$

where the index c is associated with a chosen pair of nuclei (clusters) and j is associated with a non-locality range β_j. When dealing with potentials (9), we use the experience of handling NLDOM potentials in constructing the local-equivalent adiabatic model for (d, p) reactions from Ref. [30].

3 Leading-order local-equivalent CDCC

Our aim is to find an equivalent local potential model that gives the same scattering phase shifts as the non-local model (18) does. We will follow Refs. [23, 31] to perform this. We will exploit the fact that the non-locality ranges are small. To simplify the R.H.S. of Eq. 6, we use the Perey–Buck presentation (7) of the non-local potentials V_{C_1A} and V_{C_2A}. After introducing a new variable, associated with cluster i,

$$\boldsymbol{s} = \frac{C}{C_i}\frac{A+C_i}{A+C}(\boldsymbol{R}'-\boldsymbol{R}). \tag{10}$$

Equation 5 can be rewritten as

$$\begin{aligned}(T_R + U_C(R) - E_i)\chi_i(\boldsymbol{R}) &= -\sum_j \int d\boldsymbol{s}\,d\boldsymbol{r}\,H_j(\boldsymbol{s}) \\ &\times\Big[\phi_{i'}(\boldsymbol{r})U_j^{(C_1A)}\Big(\boldsymbol{R}+\gamma_1\boldsymbol{r}+\frac{1}{2}\boldsymbol{s}\Big)\phi_i\Big(\boldsymbol{r}+\frac{A}{A+C_1}\boldsymbol{s}\Big)\chi_{i'}(\alpha_1\boldsymbol{s}+\boldsymbol{R}) \\ &+\phi_{i'}(\boldsymbol{r})U_j^{(C_2A)}\Big(\boldsymbol{R}-\gamma_2\boldsymbol{r}+\frac{1}{2}\boldsymbol{s}\Big)\phi_i\Big(\boldsymbol{r}-\frac{A}{A+C_2}\boldsymbol{s}\Big)\chi_{i'}(\alpha_2\boldsymbol{s}+\boldsymbol{R})\Big],\end{aligned} \tag{11}$$

where

$$\alpha_i = \frac{C_i}{C}\frac{A+C}{A+C_i}. \tag{12}$$

In previous $d + A$ studies [30, 31], the following step was the introduction of a new variable $\boldsymbol{x} = \boldsymbol{r} - \frac{2A}{A+2}(\boldsymbol{R}' - \boldsymbol{R})$ and neglecting $\boldsymbol{s}/(A+2)$ in the arguments of U_{nA} and U_{pA} potentials. However, a similar strategy would result in the appearance of $\frac{1}{2}[(C_2 - C_1)/C_1 \cdot A/(A+C) - C/(A+C)]\boldsymbol{s}$ in the arguments of these potentials. In the case of $C_2 \neq C_1$, this term could be important, especially for scattering of one-nucleon halo nuclei such as ^{11}Be or ^{15}C. Therefore, a different strategy is adopted here. In the term associated with cluster C_1, a new variable $\boldsymbol{y} = \gamma_1\boldsymbol{r} + \frac{1}{2}\boldsymbol{s}$ is introduced. In the term associated with cluster C_2, the integration variable $\boldsymbol{r}$ is replaced by $-\boldsymbol{r}$, followed by the introduction of $\boldsymbol{y} = \gamma_2\boldsymbol{r} + \frac{1}{2}\boldsymbol{s}$. It gives

$$\begin{aligned}(T_R + U_C(R) - E_i)\chi_i(\boldsymbol{R}) &= -\sum_{i'}\sum_c\sum_j \pi_{ii'}^{(c)}\int d\boldsymbol{s}\,d\boldsymbol{y}\,H_j(\boldsymbol{s}) \\ &\times\phi_{i'}\Big(\gamma_c^{-1}\boldsymbol{y}-\frac{1}{2\gamma_c}\boldsymbol{s}\Big)U_j^{(c)}(\boldsymbol{y}+\boldsymbol{R})\phi_i(\gamma_c^{-1}\boldsymbol{y}-\beta_c\boldsymbol{s})\chi_{i'}(\alpha_c\boldsymbol{s}+\boldsymbol{R}),\end{aligned} \tag{13}$$

where

$$\begin{aligned}\pi_{ii'}^{(c)} &= 1 \text{ for } \quad c = C_1 \\ &= (-)^{l_i+l_{i'}} \text{ for } \quad c = C_2,\end{aligned} \tag{14}$$

$$\beta_c = \frac{1}{2\gamma_c} - \frac{A}{A+C_c}. \tag{15}$$

Because of the short range of $H_j(s)$, the wave function $\chi_{i'}(\alpha\boldsymbol{s}+\boldsymbol{R})$ can be represented by the leading-order expansion that retains only spherical components in $\boldsymbol{s}$ (see [31]):

$$\chi_{i'}(\alpha_c\boldsymbol{s}+\boldsymbol{R}) \approx \sum_{n=0}^{n_{\max}}\gamma_n(\alpha_c s)^{2n}T_R^n\chi_{i'}(\boldsymbol{R}), \tag{16}$$

in which

$$\gamma_n = \frac{(-)^n}{n!\,(2n+1)!!}\left(\frac{\mu}{\hbar^2}\right)^n, \tag{17}$$

where μ is the reduced mass of $A + C$ (not to be confused with dimensionless reduced mass number μ_C of the previous section). Then, the coupled system of equations takes the form

$$\begin{aligned}(T_R + U_C(R) - E_i)\chi_i(\boldsymbol{R}) &= -\sum_{i'}\sum_{n=0}^{n_{\max}}\sum_c\sum_j \pi_{ii'}^{(c)}\int d\boldsymbol{y}\,U_j^{(c)}(\boldsymbol{y}+\boldsymbol{R}) \\ &\times\gamma_n\alpha_c^{2n}\Big[\int d\boldsymbol{s}\,s^{2n}H_j(\boldsymbol{s})\phi_i\Big(\gamma_c^{-1}\boldsymbol{y}-\frac{1}{2\gamma_c}\boldsymbol{s}\Big)\phi_{i'}(\gamma_c^{-1}\boldsymbol{y}-\beta_c\boldsymbol{s})\Big] \\ &\times T_R^n\chi_{i'}(\boldsymbol{R}) = -\sum_{i'}\sum_{n=0}^{n_{\max}}\gamma_n U_{ii'}^{(n)}(\boldsymbol{R})T_R^n\chi_{i'}(\boldsymbol{R}),\end{aligned} \tag{18}$$

where

$$\begin{aligned}U_{ii'}^{(n)}(\boldsymbol{R}) &= \sum_c\sum_j \pi_{ii'}^{(c)}\alpha_c^{2n}\int d\boldsymbol{y}\,U_j^{(c)}(\boldsymbol{y}+\boldsymbol{R}) \\ &\times\int d\boldsymbol{s}\,s^{2n}H_j(\boldsymbol{s})\phi_i\Big(\gamma_c^{-1}\boldsymbol{y}-\frac{1}{2\gamma_c}\boldsymbol{s}\Big)\phi_{i'}(\gamma_c^{-1}\boldsymbol{y}-\beta_c\boldsymbol{s}).\end{aligned} \tag{19}$$

Equation 18 could be rewritten in the following form:

$$T_R\chi_i(\boldsymbol{R}) = -\sum_{i'}\Big[(E_{i'} - U_C(R))\delta_{ii'} - \sum_n \gamma_n U_{ii'}^{(n)}(\boldsymbol{R})T_R^n\Big]\chi_{i'}(\boldsymbol{R}). \tag{20}$$

Then, imposing the requirement that the local-equivalent coupling potentials $U_{ii'}^{\rm loc}$ satisfy

$$(T_R + U_C(R) - E_i)\chi_i(\boldsymbol{R}) = -\sum_{i'} U^{\rm loc}_{ii'}(\boldsymbol{R})\chi_{i'}(\boldsymbol{R}), \tag{21}$$

we obtain a system of the transcendental matrix equations

$$f^{(0)}_{ii'} - (E_i - U_C)\delta_{ii'} + \sum_k \left(f^{(1)}_{ik} + \delta_{ik}\right)X_{ki'} + \sum_{kl} f^{(2)}_{ik} X_{kl} X_{li'} + \cdots = 0, \tag{22}$$

for

$$X_{ii'} = (E_{i'} - U_C)\delta_{ii'} - U^{\rm loc}_{ii'}, \tag{23}$$

in which $f^{(n)}_{ij} = \gamma_n U^{(n)}_{ii'}$. The system of Eq. 22 could be solved using the Newton method, as was solved in [23], and then, $U^{\rm loc}_{ii'}$ could be read into a CDCC reaction code such as FRESCO [32]. The continuum bins can have different values of orbital momentum. The partial wave decomposition of $U^{\rm loc}_{ii'}$ for general orbital momentum for cluster scattering is presented in Appendix.

4 Application to ^{6}Li scattering

We apply the aforementioned formalism to ^{6}Li+^{120}Sn scattering at two ^{6}Li incident energies, 27 MeV and 60 MeV, near and above the Coulomb barrier, respectively. ^{6}Li has a well-developed $\alpha - d$ cluster structure due to its small deuteron separation energy of 1.47 MeV. Since a non-local potential for α-d scattering is not available, to describe the continuum states of the ^{6}Li projectile, we used a local model with the same potential as in [33] to generate α-d continuum bins. This model describes the α-d s-wave phase shifts and reproduces the experimental excitation energy and width of the 3^+ resonance (E^* = 2.186 MeV) of ^{6}Li. The ^{6}Li+^{120}Sn study around the Coulomb barrier in [33] has shown that this low-energy resonance in the d-wave continuum plays an important role. Therefore, the CDCC expansion considered a basis with $l_{\alpha d} = 0$ and 2. For the d-wave component, the continuum wave functions were weighted by the T-matrix in order to better describe the resonance [32]. The calculations have been performed, ignoring the spin of the deuteron.

To calculate the couplings potentials $U_{ii'}(\boldsymbol{R})$, we used six bins for each α-d partial wave, which was deemed sufficient. The maximum α-d energy $E_{\alpha d}$ was 30 MeV for the calculation at 60 MeV since the contribution of the last bin to the breakup cross section was very small. As for the calculation at 27 MeV, the maximum value of only 6 MeV was possible due to instability of calculations with higher $E_{\alpha d}$. Variations of the maximum of $E_{\alpha d}$ lead to differences in the elastic cross section of less than 4% in the whole angular range. Convergence of the cross sections was reached by varying the matching radius R_m and maximum total angular momentum J. The optimal value R_m = 150 fm was obtained for both ^{6}Li incident energies, while the maximum total angular momentum J was 300 and 100 for ^{6}Li energies of 60 and 27 MeV, respectively.

For α-^{120}Sn and d-^{120}Sn optical potentials, we used the Sao Paulo potential (SPP) [26–28]. This potential is given by Eqs 7, 8 with the non-locality parameter $\beta = 4\hbar/(\mu_C c)$, chosen the same as in [28]. The SPP uses for $U_i(X)$ the double-folding model both for real and imaginary parts, assuming that they are proportional. The two-point Fermi distribution [28] was chosen for model density of ^{120}Sn. The deuteron density was taken from the systematics found in [28], while that for the α-particle was a sum of Gaussians taken from [34]. For the imaginary part, we used the standard renormalization coefficient

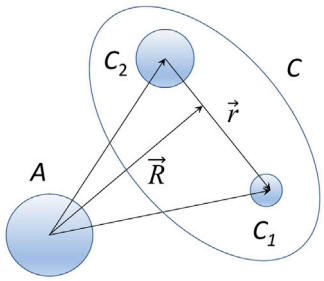

FIGURE 1
Three-body $C_1 + C_2 + A$ system associated with scattering of a two-cluster nucleus $C = C_1 + C_2$ from the target A.

0.78. The local-equivalent potential of SPP (LESPP) is obtained by solving the transcendental equation [28]

$$V_{LE}(R,E) = V_F(R) e^{-\frac{\mu\beta^2}{2\hbar^2}(E - V_C(R) - V_{LE}(R,E))}. \tag{24}$$

The solution is energy-dependent. All three-body models employing optical potentials use them only at a chosen fixed energy equal to a certain fraction of the projectile energy E. For example, in $d - A$ scattering, this would be half the incoming deuteron energy for nucleon–target potential. For cluster scattering, the fixed energy of the $C_i - A$ potential is proportional to its mass, $E_i = \frac{C_i}{C_1+C_2}E$. We compare the standard CDCC calculations with LESPP to those obtained in LECDCC developed in this work. We made sure that for $\beta \to 0$, they coinside with standard local folding potential calculations when breakup is neglected.

Figure 2 shows selected coupling potentials calculated in standard CDCC with LESPP and in LECDCC. The $U^{\rm LESPP}_{\rm gs-gs}(R)$ and $U^{\rm LECDCC}_{\rm gs-gs}(R)$ couplings, shown in Figures 2A, B for ^{6}Li incident energies of 27 and 60 MeV, respectively, are very similar in the surface region, around $R \approx$ 8–12 fm. At R = 0 fm, their real parts differ by 4% at 27 MeV and by 19% at 60 MeV, but imaginary parts of $U^{\rm LECDCC}_{\rm gs-gs}(0)$ are more than twice smaller than those of $U^{\rm LESPP}_{\rm gs-gs}(0)$. A similar situation occurs for diagonal couplings $U^{\rm LECDCC}_{\rm ex-ex}(R)$ between d-wave bin states with the first 2^+ resonance (see Figure 2C). We have only plotted it for the ^{6}Li energy of 60 MeV because the differences there are expected to be higher. Non-diagonal couplings between these states, $U^{\rm LESPP}_{\rm ex-gs}(R)$ and $U^{\rm LECDCC}_{\rm ex-gs}(R)$, are also very similar at the surface. However, the difference in the internal region is more significant.

Despite a significant difference in the coupling potentials $U_{ii'}(R)$ within the short range of the optical potentials, the elastic scattering angular distributions calculated in LECDCC turned out to be very similar to those obtained in standard CDCC with LESPP. Therefore, we only show their ratio in Figure 3. For an incident energy of 27 MeV, the difference between the two approaches does not exceed 4% in the whole angular range. At 60 MeV, numerical noise has not allowed us to unambiguously determine this ratio at angles larger than 90°. Below 90°, the difference between LECDCC and LESPP does not exceed 8%. We also observe some oscillations in the LECDCC/LESPP ratio, resulting from tiny oscillations in both these differential cross sections, which are slightly out of phase. These oscillations are

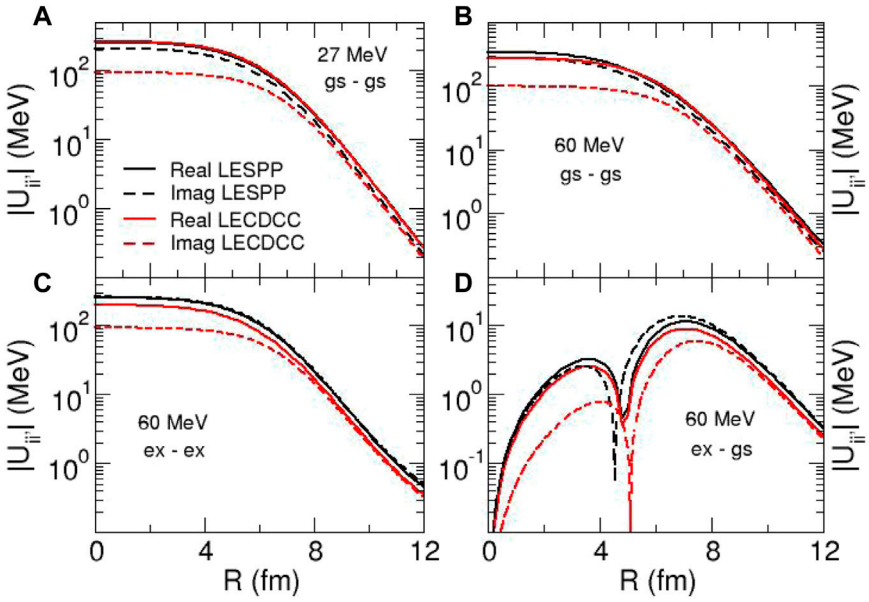

FIGURE 2
λ = 0 LECDCC diagonal **(A–C)** and non-diagonal **(D)** coupling potentials for ^{120}Sn+^{6}Li at an incident energy of 27 MeV **(A)** and 60 MeV **(B–D)**. The excited state corresponds to the bin state with the first 2^+ resonance.

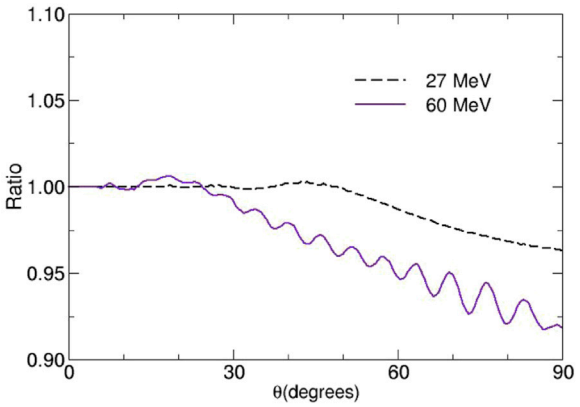

FIGURE 3
Ratio of the differential cross section for ^{6}Li + ^{120}Sn elastic scattering calculated in LECDCC to standard CDCC calculations with a local SPP potential at 27 and 60 MeV.

caused by a small near-far-side interference, which results in a small Fraunhofer diffraction pattern.

The breakup cross sections are more strongly influenced by non-locality. The differential *s*-wave, *d*-wave, and total breakup cross sections are shown in Figure 4. One can see that these cross sections are dominated by the *d*-wave breakup and that treating non-locality at the leading order in CDCC increases these cross sections. At an incident energy of 27 MeV, this increase is most noticeable at the main peak around 40°, while at 60 MeV, the increase occurs at most angles. The LECDCC/LESPP ratio for angle-integrated breakup cross sections is shown in Figure 5 as a function of bin energy. One can see that the non-locality effect can reach 20% in the breakup cross sections for both incident energies for higher energy bins. Since this effect is bin-dependent, it is possible that the non-locality effect can strongly depend on kinematic conditions of breakup observation.

Finally, we found that the total breakup cross sections $\sigma_{\rm bu}$ and reaction cross sections $\sigma_{\rm reac}$ are less affected by non-local effects. These cross sections are collected in Table 1, showing about 0.1% difference in $\sigma_{\rm reac}$ between LESPP and LECDCC calculations. For $\sigma_{\rm bu}$, this difference is 3% and 5% for 27 and 60 MeV, respectively.

The non-local effects in ^{6}Li elastic scattering turned to be much smaller than those associated with deuteron scattering — the simplest nucleus with a cluster structure. We have identified the reason why this happens, which is the Coulomb barrier (for smaller angles) and strong absorption that make the reaction mechanism less sensitive to the interactions in the nuclear interior. Since both LESPP and

TABLE 1 $d + \alpha$ **breakup and absorption cross sections for the ^{6}Li +^{120}Sn reaction calculated in CDCC with the local-equivalent SPP (LESPP) and in LECDCC with the non-local SPP potential.**

	$\sigma_{\rm bu}$ (mb) 60 MeV	$\sigma_{\rm reac}$ (mb) 60 MeV	$\sigma_{\rm bu}$ (mb) 27 MeV	$\sigma_{\rm reac}$ (mb) 27 MeV
LESPP	79.9	2,436	65.1	1,123
LECDCC	84.3	2,422	67.1	1,125

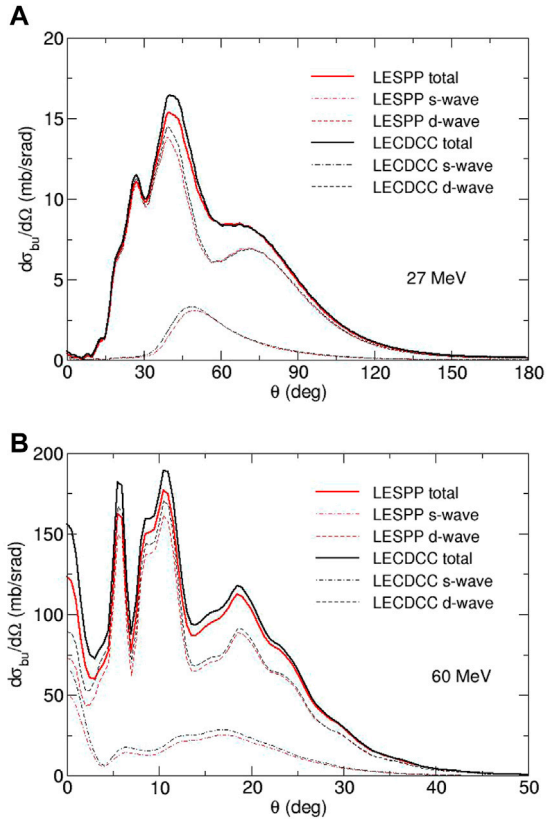

FIGURE 4
Angular distribution for breakup using LECDCC and standard CDCC calculations with the local-equivalent SPP potential (LESPP). **(A)** Angular distribution for breakup in LECDCC (black curves) and standard CDCC calculations with local SPP potential (red curves) for ^{6}Li + ^{120}Sn scattering at 27 MeV (circles). Dashed, dot-dashed, and solid curves correspond to *d*-wave, *s*-wave, and total breakup, respectively. **(B)** Same for the ^{6}Li incident energy of 60 MeV.

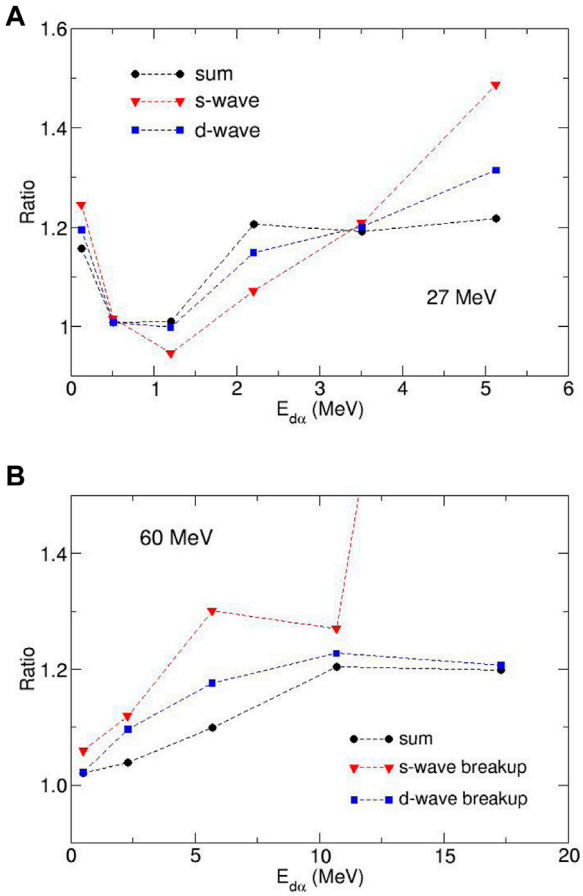

FIGURE 5
Ratio of the breakup cross section calculated in LECDCC to standard CDCC calculations with local-equivalent SPP potential (LESPP) for each bin. **(A)** Ratio of breakup cross sections for ^{6}Li + ^{120}Sn scattering at 27 MeV (circles). The ratios for *s*- and *d*-wave breakup are shown by triangles and squares, respectively. **(B)** Same for the ^{6}Li incident energy of 60 MeV. The *s*-wave ratio at the last point is equal to three.

LECDCC potentials are very similar at the surface, the cross sections should be similar as well. We repeated both calculations reducing the imaginary part by 50% for an ^{6}Li incident energy of 60 MeV. The difference between LESPP and LECDCC has increased to 20% at 60° and become an order of magnitude greater after 100°. However, the elastic cross sections in this angular range are small. The difference in breakup cross sections exceeded 20% after $E_{\alpha d}$ = 5 MeV. The angular distribution for the breakup cross section also presents larger differences with a reduced absorption, of ~10%–20% for small angles and larger than 50% for angles larger than 60°. The difference in reaction cross sections remains small.

5 Summary and conclusion

To assess the validity of a standard approach which replaces non-local optical potentials by their local equivalents in cluster scattering calculations, we developed a leading-order method to include the non-locality of pairwise optical potentials into a three-body Hamiltonian describing cluster scattering. This resulted in a coupled system of transcendental equations for local-equivalent coupling potentials that could be fed into standard CDCC equations. The application to ^{6}Li +^{120}Sn scattering at the incident energy of 27 and 60 MeV has shown that elastic scattering is not much affected by non-locality, while breakup cross sections in some kinematical regions could increase the differential cross sections up to 20%.

Both elastic and breakup observables are determined by scattering phase shifts in all CDCC channels, which determine asymptotics of the channel wave functions. The LECDCC has been constructed to provide phase-equivalent solutions to non-local problems. At small distances, the LECDCC local CDCC channel functions should differ more strongly from each other. Therefore, the cross sections of other reactions that are more sensitive to internal parts of the three-body wave function than the projectile breakup, such as transfer reactions, could be more affected by the non-locality.

Using non-local optical potentials to describe various nuclear reactions induced by nuclei with the pronounced cluster structure requires further development of techniques to solve the three-body Schrödinger equation. For such reactions, beyond-leading-order effects could be very important. It is

well-known that in the region of strong nuclear interaction, a two-body scattering wave function, obtained in a non-local model, is smaller than that obtained in the leading-order local-equivalent model by a quantity called the Perey factor [35]. The Perey factor also appears in the three-body model with velocity-dependent potentials [36]. However, incorporating the Perey effect into the LECDCC scheme is not easy. Therefore, it would make sense to try solving the non-local CDCC exactly. The obstacle on this path is the absence of formalism for non-local CDCC couplings. The easiest way to develop such formalism is to extend the non-local adiabatic model proposed for (d, p) in [37], but it would be applicable only to non-localities of the Perey–Buck type. Optical potentials coming from *ab initio* calculations have a more complicated structure, and including them into the CDCC approach requires a major effort, which will become an important task for future research.

Finally, this paper considered only the processes in which the target A was not excited. Many experiments with weakly bound projectiles involve nuclei, both the target and projectile, with low-lying excited states that play an important role in the reaction mechanism. It has just been demonstrated that using non-local optical potentials with core excitation achieves a considerably more successful description of the experimental data on (d, p) reactions as compared to previous studies with local potentials [38]. When nuclear excitations are explicitly included in coupled-channel calculations, the imaginary part that describes absorption is usually reduced. One can expect that non-local effects could be stronger in coupled-channel calculations with reduced absorption. The LECDCC introduced here could be readily extended to include core excitations to study these effects.

Data availability statement

The original contributions presented in the study are included in the article/Supplementary Material, further inquiries can be directed to the corresponding author.

Author contributions

NT developed the reaction formalism presented in this work and wrote the article. MG-R developed the codes required for its implementation, run the calculations that produced the results shown, and contributed to writing. All authors contributed to the article and approved the submitted version.

Funding

This work was supported by the United Kingdom Science and Technology Facilities Council (STFC) under Grant No. ST/V001108/1 and by MCIN/AEI/10.13039/501100011033 (also known as Agencia Estatal de Investigacion) under Project PID2020-114687GB-I00; by MCIN/AEI/10.13039/501100011033 and "European Union Next-Generation EU/PRTR" under Grant: IJC2020-043878-I; and by Consejeria de Economia, Conocimiento, Empresas y Universidad, Junta de Andalucia, and "ERDF-A Way of Making Europe" under Project P20_01247.

Conflict of interest

The authors declare that the research was conducted in the absence of any commercial or financial relationships that could be construed as a potential conflict of interest.

Publisher's note

References

1. Freer M, Merchant AC. Developments in the study of nuclear clustering in light even - even nuclei. *J Phys G: Nucl Part Phys* (1997) 23:261–323. doi:10.1088/0954-3899/23/3/002

2. Maruhn JA, Kimura M, Schramm S, Reinhard P-G, Horiuchi H, Tohsaki A. α-cluster structure and exotic states in a self-consistent model for light nuclei. *Phys Rev C* (2006) 74:044311. doi:10.1103/physrevc.74.044311

3. Tanihata I, Hamagaki H, Hashimoto O, Shida Y, Yoshikawa N, Sugimoto K, et al. Measurements of interaction cross sections and nuclear radii in the lightp-shell region. *Phys Rev Lett* (1985) 55:2676–9. doi:10.1103/physrevlett.55.2676

4. Kubono S. Nuclear clustering aspects in astrophysics. In: GS Anagnostatos W von Oertzen, editors. *Atomic and nuclear clusters*. Berlin, Heidelberg: Springer (1995). doi:10.1007/978-3-642-79696-8_16

5. Kolata JJ, Guimarães V, Aguilera EF. Elastic scattering, fusion, and breakup of light exotic nuclei. *Eur Phys J A* (2016) 52:123. doi:10.1140/epja/i2016-16123-1

6. Bazin D, Becker K, Bonaiti F, Elster C, Fossez K, Frederico T. Perspectives on few-body cluster structures in exotic nuclei. *Few-body Syst* (2023) 64:25. doi:10.1007/s00601-023-01794-0

7. Feshbach H. Unified theory of nuclear reactions. *Ann Phys* (1958) 5:357–90. doi:10.1016/0003-4916(58)90007-1

8. Hebborn C, Nunes FM, Potel G, Dickhoff WH, Holt JW, Baker RB, et al. Optical potentials for the rare-isotope beam era. *J Phys G* (2023) 50:060501. doi:10.1088/1361-6471/acc348

9. Perey F, Buck B. A non-local potential model for the scattering of neutrons by nuclei. *Nucl Phys* (1962) 32:353–80. doi:10.1016/0029-5582(62)90345-0

10. Fiedeldey H. The equivalent local potential and the Perey effect. *Nucl Phys* (1966) 77:149–56. doi:10.1016/0029-5582(66)90682-1

11. Descouvemont P. The *R*-matrix theory. *D Baye Rep Prog Phys* (2010) 73:036301. doi:10.1088/0034-4885/73/3/036301

12. Michel N. A simple and efficient numerical scheme to integrate non-local potentials. *Eur Phys J A* (2009) 42:523. doi:10.1140/epja/i2008-10738-7

13. Rawitscher GH. Solution of the schrödinger equation containing a perey–buck nonlocality. *Nucl Phys A* (2012) 886:1–16. doi:10.1016/j.nuclphysa.2012.05.001

14. Arellano HF, Blanchon G. Exact scattering waves off nonlocal potentials under Coulomb interaction within Schrödinger's integro-differential equation. *Phys Lett B* (2019) 789:256–61. doi:10.1016/j.physletb.2018.12.004

15. Timofeyuk NK, Johnson RC. Theory of deuteron stripping and pick-up reactions for nuclear structure studies. *Prog Part Nucl Phys* (2020) 111:103738. doi:10.1016/j.ppnp.2019.103738

16. Doleschall P. Phenomenological non-local nucleon-nucleon interactions and the neutron-deuteron elastic scattering. *Few-body Syst* (1998) 23:149–86. doi:10.1007/s006010050069

17. Doleschall P, Papp Z. p–dscattering with a nonlocal nucleon-nucleon potential below the breakup threshold. *Phys Rev C* (2005) 72:044003. doi:10.1103/physrevc.72.044003

18. Viviani M, Girlanda L, Kievsky A, Marcucci LE, Rosati S. Bound and scattering states with non-local potentials. *Nucl Phys* (2007) A790:46–51c. doi:10.1016/j.nuclphysa.2007.03.054

19. Marcucci LE, Kievsky A, Girlanda L, Rosati S, Viviani M. N–delastic scattering using the hyperspherical harmonics approach with realistic local and nonlocal interactions. *Phys Rev C* (2009) 80:034003. doi:10.1103/physrevc.80.034003

20. Deltuva A. Three-body direct nuclear reactions: Nonlocal optical potential. *Phys Rev* (2009) C79:021602. doi:10.1103/physrevc.79.021602

21. Deltuva A. Deuteron stripping and pickup involving halo nuclei Be-11 and C-15. *Phys Rev C* (2009) 9:054603. doi:10.1103/PhysRevC.79.054603

22. Deltuva A, Jurčiukonis D. Calculation of three-body nuclear reactions with angular-momentum and parity-dependent optical potentials. *Phys.Rev C* (2016) 94:054619. doi:10.1103/physrevc.94.054619

23. Gómez-Ramos M, Timofeyuk NK. Reduced sensitivity of the (d,p) cross sections to the deuteron model beyond the adiabatic approximation. *Phys Rev C* (2018) 98:011601. doi:10.1103/physrevc.98.011601

24. Rawitscher GH. Effect of deuteron breakup on elastic deuteron - nucleus scattering. *Phys Rev C9* (1974) 9:2210–29. doi:10.1103/physrevc.9.2210

25. Austern N, Iseri Y, Kamimura M, Kawai M, Rawitscher G, Yahiro M. Continuum-discretized coupled-channels calculations for three-body models of deuteron-nucleus reactions. *Phys Rep* (1987) 154:125–204. doi:10.1016/0370-1573(87)90094-9

26. Cândido Ribeiro MA, Chamon LC, Pereira D, Hussein MS, Galetti D. Pauli nonlocality in heavy-ion rainbow scattering: A further test of the folding model. *Phys Rev Lett* (1997) 78:3270–3. doi:10.1103/physrevlett.78.3270

27. Chamon LC, Pereira D, Hussein MS, Candido Ribeiro MA, Galetti D. Nonlocal description of the nucleus-nucleus interaction. *Phys Rev Lett* (1997) 79:5218–21. doi:10.1103/physrevlett.79.5218

28. Chamon LC, Carlson BV, Gasques LR, Pereira D, De Conti C, Alvarez MAG, et al. Toward a global description of the nucleus-nucleus interaction. *Phys Rev C* (2002) 66:014610. doi:10.1103/physrevc.66.014610

29. Mahzoon MH, Charity RJ, Dickhoff WH, Dussan H, Waldecker SJ. Forging the link between nuclear reactions and nuclear structure. *Phys Rev Lett* (2014) 112:162503. doi:10.1103/physrevlett.112.162503

30. Waldecker SJ, Timofeyuk NK. Implications for(d,p)reaction theory from nonlocal dispersive optical model analysis ofCa40(d,p)Ca41. *Phys Rev C* (2016) 94:034609. doi:10.1103/physrevc.94.034609

31. Timofeyuk NK, and Johnson RC. Nonlocality in the adiabatic model of A(d, p)B reactions. *Phys Rev C* (2013) 87:064610. doi:10.1103/PhysRevC.87.064610

32. Thompson IJ. Coupled reaction channels calculations in nuclear physics. *Comput Phys Rep* (1988) 7:167. doi:10.1016/0167-7977(88)90005-6

33. Zagatto VAB, Gonçalves BR, Junior M, et al. Energy dependent optical potential for reactions involving. *Phys Rev C* (2022) 106:014622. doi:10.1103/PhysRevC.107.044604

34. De Vries H, De Jager CW, De Vries C. Nuclear charge-density-distribution parameters from elastic electron scattering. *Data Nucl Data Tables* (1987) 36:495–536. doi:10.1016/0092-640x(87)90013-1

35. Perey F *Direct interactions and nuclear reaction mechanisms*. New York: Gordon & Breach (1964). p. 125.

36. Gómez-Ramos M, Timofeyuk NK. Perey-effect in continuum-discretized coupled-channel description of (*d, p*) reactions. J *Phys G: Nucl Part Phys* (2019) 46:085102. doi:10.1088/1361-6471/ab25c5

37. Bailey GW, Timofeyuk NK, Tostevin JA. Nonlocal nucleon-nucleus interactions in (d,p) reactions: Role of the deuteron D state. *Phys Rev C* (2017) 95:024603. doi:10.1103/physrevc.95.024603

38. Deltuva A, Jurčiukonis D. Nonlocal optical potential with core excitation in ^{10}Be (d, *p*)^{11} Be and ^{11}Be (*p*, d)^{10} Be reactions. *Phys Lett B* (2023) 840:137867. doi:10.1016/j.physletb.2023.137867

Appendix

Three-body Schrödinger equation in laboratory and centre-of-mass frames

In a fixed frame of reference where experimental cross-sections are measured, the laboratory frame, the Schrödinger equation for the $C_1 + C_2 + A$ wave function $\Psi_{\rm lab}(\boldsymbol{r}_{C_1}, \boldsymbol{r}_{C_2}, \boldsymbol{r}_A)$ of the $C_1 + C_2 + A$ system with non-local $C_1 - A$, $C_2 - A$ and $C_1 - C_2$ interactions is written as

$$\begin{aligned}
&(T_{C_1} + T_{C_2} + T_A - E_3)\Psi_{\rm lab}(\boldsymbol{r}_{C_1}, \boldsymbol{r}_{C_2}, \boldsymbol{r}_A) = -\int d\boldsymbol{r}'_{C_1}\, d\boldsymbol{r}'_{C_2}\, d\boldsymbol{r}'_A \\
&\times \left[\delta\left(\boldsymbol{r}_{C_2} - \frac{C_1\boldsymbol{r}_{C_1} + A\boldsymbol{r}_A}{A + C_1} - \boldsymbol{r}'_{C_2} + \frac{C_1\boldsymbol{r}'_{C_1} + A\boldsymbol{r}'_A}{A + C_1}\right) V_{C_1A}(\boldsymbol{r}'_{C_1} - \boldsymbol{r}'_A, \boldsymbol{r}_{C_1} - \boldsymbol{r}_A)\right. \\
&+ V_{C_2A}(\boldsymbol{r}'_{C_2} - \boldsymbol{r}'_A, \boldsymbol{r}_{C_2} - \boldsymbol{r}_A)\,\delta\left(\boldsymbol{r}_{C_1} - \frac{C_2\boldsymbol{r}_{C_2} + A\boldsymbol{r}_A}{A + C_2} - \boldsymbol{r}'_{C_1} + \frac{C_1\boldsymbol{r}'_{C_2} + A\boldsymbol{r}'_A}{A + C_2}\right) \\
&\left. + V_{C_1C_2}(\boldsymbol{r}'_{C_1} - \boldsymbol{r}'_{C_2}, \boldsymbol{r}_{C_1} - \boldsymbol{r}_{C_2})\,\delta\left(\boldsymbol{r}_A - \frac{C_1\boldsymbol{r}_{C_1} + C_2\boldsymbol{r}_{C_2}}{C_1 + C_2} - \boldsymbol{r}'_A + \frac{C_1\boldsymbol{r}'_{C_1} + C_2\boldsymbol{r}'_{C_2}}{C_1 + C_2}\right)\right] \\
&\times \delta\left(\frac{C_1\boldsymbol{r}_{C_1} + C_2\boldsymbol{r}_{C_2} + A\boldsymbol{r}_A}{A + C_1 + C_2} - \frac{C_1\boldsymbol{r}'_{C_1} + C_2\boldsymbol{r}'_{C_2} + A\boldsymbol{r}'_A}{A + C_1 + C_2}\right)\Psi_{\rm lab}(\boldsymbol{r}'_{C_1}, \boldsymbol{r}'_{C_2}, \boldsymbol{r}'_A),
\end{aligned} \tag{25}$$

where E_3 is the three-body energy in the laboratory system. Separating the centre-of-mass motion,

$$\Psi_{\rm lab}(\boldsymbol{r}_{C_1}, \boldsymbol{r}_{C_2}, \boldsymbol{r}_A) = \phi_{\rm cm}\left(\frac{C_1\boldsymbol{r}_{C_1} + C_2\boldsymbol{r}_{C_2} + A\boldsymbol{r}_A}{A + C_1 + C_2}\right)\Psi\left(\boldsymbol{r}_{C_1} - \boldsymbol{r}_{C_2}, \boldsymbol{r}_A - \frac{C_1\boldsymbol{r}_{C_1} + C_2\boldsymbol{r}_{C_2}}{C_1 + C_2}\right), \tag{26}$$

then introducing variables

$$\begin{aligned}
\boldsymbol{r} &= \boldsymbol{r}_{C_1} - \boldsymbol{r}_{C_2}, \\
\boldsymbol{R} &= \frac{C_1\boldsymbol{r}_{C_1} + C_2\boldsymbol{r}_{C_1}}{C_1 + C_2} - \boldsymbol{r}_A, \\
\boldsymbol{R}_{\rm cm} &= \frac{C_1\boldsymbol{r}_{C_1} + C_2\boldsymbol{r}_{C_2} + A\boldsymbol{r}_A}{A + C_1 + C_2}
\end{aligned} \tag{27}$$

and integrating over $\boldsymbol{r}'$ and $\boldsymbol{R}'_{cm}$ in the r.h.s of Eq. (25) we get Eq. (2).

Partial wave decomposition of coupling potentials $U^{(n)}_{ii'}(\boldsymbol{R})$

In the case of non-zero orbital momenta of continuum bins we use, assuming zero spins for clusters C_1 and C_2, we have

$$\phi_i(a\boldsymbol{y} - b\boldsymbol{s}) = \sqrt{4\pi}\sum_{\lambda_1\lambda_2}\phi^{l_i}_{\lambda_1\lambda_2}(ay, bs)\left[Y_{\lambda_1}(\hat{y}) \times Y_{\lambda_2}(\hat{s})\right]_{l_im_i} \tag{28}$$

Then for spherical optical potentials

$$\begin{aligned}
U^{(n)}_{ii'}(\boldsymbol{R}) &= 4\pi\sum_c\sum_j \pi^{(c)}_{ii'}\alpha^{2n}_c \sum_{\lambda\lambda_1\lambda_2\lambda'_1}(-)^{\lambda}Y_{\lambda\mu}(\hat{R})\int_0^\infty dy\, y^2 U^{(c)}_{j,\lambda}(y, R) \\
&\times \int_0^\infty ds\, s^{2+2n}H_j(s)\phi^{l_i}_{\lambda_1\lambda_2}\left(\gamma_c^{-1}y, \frac{1}{2\gamma_c}s\right)\phi^{l'_i}_{\lambda'_1\lambda_2}(\gamma_c^{-1}y, \beta_c s) \\
&\times \sum_{\mu_1\mu_2\mu}(\lambda_1\mu_1\lambda_2\mu_2|l_im_i)(\lambda'_1\mu'_1\lambda_2\mu_2|l'_im'_i)(\lambda_1 - \mu_1\lambda'_1\mu'_1|\lambda\mu)(\lambda_1 0\lambda'_1 0|\lambda 0)\frac{\hat{\lambda}_1\hat{\lambda}'_1}{\sqrt{4\pi}\hat{\lambda}}(-)^{\mu_1} \\
&= \sqrt{4\pi}\sum_{\lambda\mu}(\lambda\mu l_im_i|l'_im'_i)Y_{\lambda\mu}(\hat{R})\sum_c \pi^{(c)}_{ii'}\alpha^{2n}_c\int_0^\infty dy\, y^2\left[\sum_j U^{(c)}_{j,\lambda}(y, R)f^{n,\lambda}_{(j)l_il'_i}(y, R)\right],
\end{aligned} \tag{29}$$

where

$$\begin{aligned}
f^{n,\lambda}_{(j)l_il'_i}(y, R) &= \sum_{\lambda_1\lambda_2\lambda'_1}(-)^{\lambda'_1}\hat{\lambda}_1\hat{\lambda}\hat{l}_i(\lambda_1 0\lambda'_1 0|\lambda 0)W(\lambda\lambda_1 l'_i\lambda_2; \lambda'_1 l_i) \\
&\times \int_0^\infty ds\, s^{2+2n}H_j(s)\phi^{l_i}_{\lambda_1\lambda_2}\left(\gamma_c^{-1}y, \frac{1}{2\gamma_c}s\right)\phi^{l'_i}_{\lambda'_1\lambda_2}(\gamma_c^{-1}y, \beta_c s).
\end{aligned} \tag{30}$$

Finally, the radial part of the partial wave decomposition of the continuum bin is

$$\begin{aligned}
\phi^l_{\lambda_1\lambda_2}(x, y) = \sum_{\Lambda l_x l_y}(-)^{\lambda_2}&\sqrt{\frac{(2l+1)!}{(2l_x)!(2l_y)!}}(l_x 0\Lambda 0|\lambda_1 0) \\
&(l_y 0\Lambda 0|\lambda_2 0)W(\lambda_1\Lambda l l_y; l_x\lambda_2)x^{l_x}y^{l_y}\phi^{(l)}_\Lambda(x, y)
\end{aligned} \tag{31}$$

where $l_x + l_y = l$ and

$$\phi^{(l)}_\Lambda(x, y) = \frac{2\Lambda + 1}{2}\int_{-1}^{1} d\mu P_\Lambda(\mu)(x^2 - 2\mu xy + y^2)^{-l/2}\phi_l\left(\sqrt{x^2 - 2\mu xy + y^2}\right) \tag{32}$$

where $\phi_l(r)$ is the radial part of the continuum bin in the partial wave l. The integration variable s, chosen in (29), uses the short-range nature of $H(s)$, which makes accurate evaluation of (30) easy. Then the integral over dy is similar to a standard CDCC matrix element for which accurate numerical methods are in place.